

# Dual-Band 4-Port Vivaldi MIMO Antenna for 5G mmWave Applications at 28/39 GHz

Golla Ramyasree\* and Nelaturi Suman

**Abstract**—A compact new dual band 4-port Vivaldi MIMO (Multiple-Input-Multiple-Output) antenna is designed for 5G mmWave applications. The proposed MIMO antenna resonates at two frequencies 28 GHz and 39 GHz, and it has dimensions  $22 \times 22 \times 0.79 \text{ mm}^3$ . The Vivaldi structure etched on ground plane acts as a defected ground structure (DGS). The proposed antenna is fabricated on Rogers RT/duroid 5880 material having 0.79 mm thickness and 2.2 dielectric material. For high frequency and broad band applications RT/duroid material is suited to maintain low dielectric loss, and it works in high temperature places also. For the proposed four port Vivaldi MIMO antenna, the isolation between any two antenna elements is obtained below  $-21.59 \text{ dB}$ . The bandwidths achieved for two bands are 4.64 GHz (26.31–30.95 GHz) at 28 GHz resonant frequency and 2.69 GHz (38.35–41.04 GHz) at 39 GHz resonant frequency for 4-port MIMO antenna. The gain achieved at 28 GHz is 5.65 dB and at 39 GHz is 5.53 dB. It is possible to achieve MIMO performance parameters such as  $\text{ECC} < 0.003$ ,  $\text{DG} = 10$ ,  $\text{CCL} < 0.4 \text{ (bits/s/Hz)}$ ,  $\text{TARC} < -10 \text{ dB}$ , and MEG ratio is 1.01. Simulated and measured results are compared, and the antenna is designed using ansys HFSS tool.

## 1. INTRODUCTION

Nowadays 5G wireless communication systems demand compact, wide-band multiple-input-multiple-output (MIMO) antennas with improved port isolation. The MIMO antenna plays a crucial role for extending the range of the signal transmission without increasing the signal's power even while providing high efficiency, minimal delay, maximum throughput, and increased channel capacity [1]. The 5G bands are categorized as low band, mid-band, and high band. With 600 MHz to 2600 MHz of available spectrum, 5G low bands are used to cover vast distances and provide wide-area coverage. According to ITU-R specifications, 5G mid-bands, also known as FR1 (frequency range 1), offer a frequency band from 410 MHz to 7125 MHz which provides more capacity across short distances. 3.5 GHz band is the most frequently used in mid-band for the deployment of various technologies like MIMO to improve capacity. The frequency band offered by 5G high bands, commonly known as mm-Wave or FR2 (frequency range2), ranges from 24.25 GHz to 52.6 GHz. Massive MIMO can be used with these 5G high bands to improve capacity and widen the coverage area. Early on, the 28 GHz spectrum was identified and implemented by various markets, including the US, Japan, and Korea. The WRC-19 (world radio communication conference) agreed that FR2 should be widely tagged for 5G [2]. Future broadband wireless communication devices can use the mm-Wave spectrum [3].

In 1979, Gibson invented tapered slot antennas, also called Vivaldi antennas [4]. Vivaldi antennas are also considered as broadband antennas because of their larger bandwidth. The 3D models of Vivaldi antennas are commonly made available [5]. While size is a challenge when designing 3D models, printed Vivaldi antennas have been used to reduce their size complexity [6–8]. Vivaldi antennas have been

---

*Received 4 August 2023, Accepted 22 August 2023, Scheduled 12 September 2023*

\* Corresponding author: Golla Ramyasree (ramyasree.golla@gmail.com).

The authors are with Department of Electronics and Communication Engineering, VFSTR (Deemed to be University), Vadlamudi, Guntur, Andhra Pradesh, India.

used in several fields like satellites, radars, and medical applications [9–11]. 5G communications have been carried out using Vivaldi antennas [12–14, 26]. Different techniques and methodologies have been reported for dual-band 5G applications [15–28].

A planar dual-band millimeter wave  $2 \times 2$  monopole MIMO antenna 28/38 GHz is presented for future 5G communications with new radiating element [15]. A novel 28/38 GHz dual-band printed MIMO antenna is designed for 5G mobile applications with a defected ground structure (DGS) etched on partial rectangular ground plane [16]. A two-port dual-band 27/39 GHz mm-Wave MIMO antenna is suggested for 5G applications with high efficiency [17], and here two elements are arranged in opposite directions. A reconfigurable circularly polarized 28/38 GHz patch antenna for the fifth generation mobile communication systems is reported [18]. The four-port dual-band 28/38 GHz Yagi-Uda antenna has triangular reflectors and corrugated radiator for 5G mobile applications [19]. A compact 4-port dual-band 28/38 GHz diamond patch antenna is introduced for 5G wireless communications [20]. A composite patch antenna is constructed for dual-band 28/38 GHz multi-input multi-output antenna for the fifth generation mobile applications [21]. A parasitic element loaded dual-band 28/38 GHz four port MIMO antenna is proposed to enhance the isolation between antenna elements for 5G mm-Wave applications [22]. A dual-band 28/38 GHz four-port MIMO antenna is designed for mm-Wave 5G applications [23]. Here the antenna size is compact, and elements are arranged in orthogonally to improve isolation. A two-port MIMO antenna is proposed for mm-Wave 5G applications [24]. Metamaterials are used to improve the isolation between elements. A 28 GHz single band MIMO antenna is proposed for 5G mm-Wave applications [25], and DGS is employed to improve the antenna performance. A Vivaldi antenna is designed for 4G/5G wireless devices, but size is large, and the antenna is operated at three bands [26]. A 28/38 GHz two-port MIMO antenna is proposed for 5G applications [27], but size is large, and gain is also less than the proposed antenna. An antipodal Vivaldi antenna is proposed with ultra-wideband and high gain for 5G mm-Wave applications [28].

The proposed antenna is designed for dual-band 28/39 GHz 5G millimeter wave applications. The proposed antenna is less in size with large bandwidths with acceptable isolation between elements, Gain and MIMO performance characteristics are compared to the existing systems.

## 2. ANTENNA GEOMETRY

A four-port MIMO Vivaldi antenna is designed at dual-band 28 GHz and 39 GHz frequencies. Firstly, a single element Vivaldi antenna is designed at dual bands, and it has dimensions  $11 \times 11 \times 0.79 \text{ mm}^3$  as shown in Fig. 1(a). Here Vivaldi structure acts as a defected ground structure (DGS) as shown in Fig. 1(a)-ii. Using Vivaldi structure reduces the size of the antenna. Because of this Vivaldi structure or tapered curve, we can obtain more bandwidth and gain. Vivaldi (or) exponential tapered curve

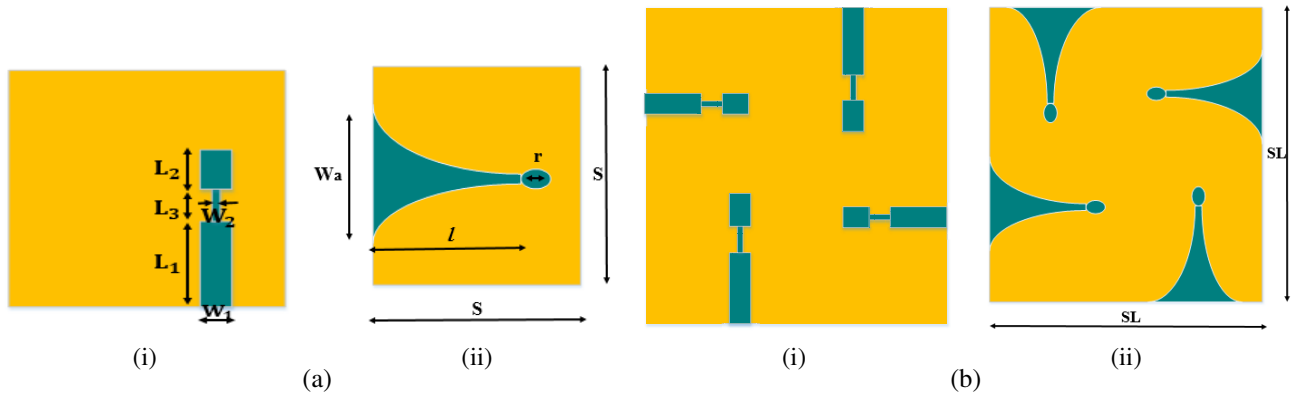


**Figure 1.** Proposed antenna geometry. (a) Single element vivaldi antenna, (i) front view, (ii) back view. (b) Four-port MIMO vivaldi antenna, (i) front view, (ii) back view. ( $Sl = 22 \text{ mm}$ ,  $S = 11 \text{ mm}$ ,  $W_a = 5 \text{ mm}$ ,  $l = 7.5 \text{ mm}$ ,  $W_1 = 1 \text{ mm}$ ,  $W_2 = 0.3 \text{ mm}$ ,  $L_1 = 5.5 \text{ mm}$ ,  $L_2 = 2 \text{ mm}$ ,  $L_3 = 1.63 \text{ mm}$  and  $r = 0.8 \text{ mm}$ ).

equation can be defined using two points  $P_1(x_1, y_1)$  and  $P_2(x_2, y_2)$  and is expressed [19] as

$$y = c_1 e^{ax} + c_2 \tag{1}$$

$$C_1 = \frac{(y_2 - y_1)}{e^{ax_2} - e^{ax_1}} \tag{2}$$

$$C_2 = \frac{(y_1 e^{ax_2} - y_2 e^{ax_1})}{e^{ax_2} - e^{ax_1}} \tag{3}$$

Here  $C_1$  and  $C_2$  are constants. ‘ $a$ ’ is the opening rate of the exponential tapered curve.

The proposed four-port Vivaldi antenna is shown in Fig. 1(b). Aperture width ( $W_a$ ) is defined by using the given formula

$$W_a = \frac{c}{f_{\min} \sqrt{\epsilon_r}} \tag{4}$$

$C$  — Speed of light,  $\epsilon_r$  — Dielectric material constant.

From Fig. 1(b) it can be observed that antenna elements are placed in orthogonally to reduce the size and improve the isolation between elements. So many parametric studies are done to get dual bands, return loss, optimal bandwidth, and isolation of the proposed antenna as seen in Fig. 2.

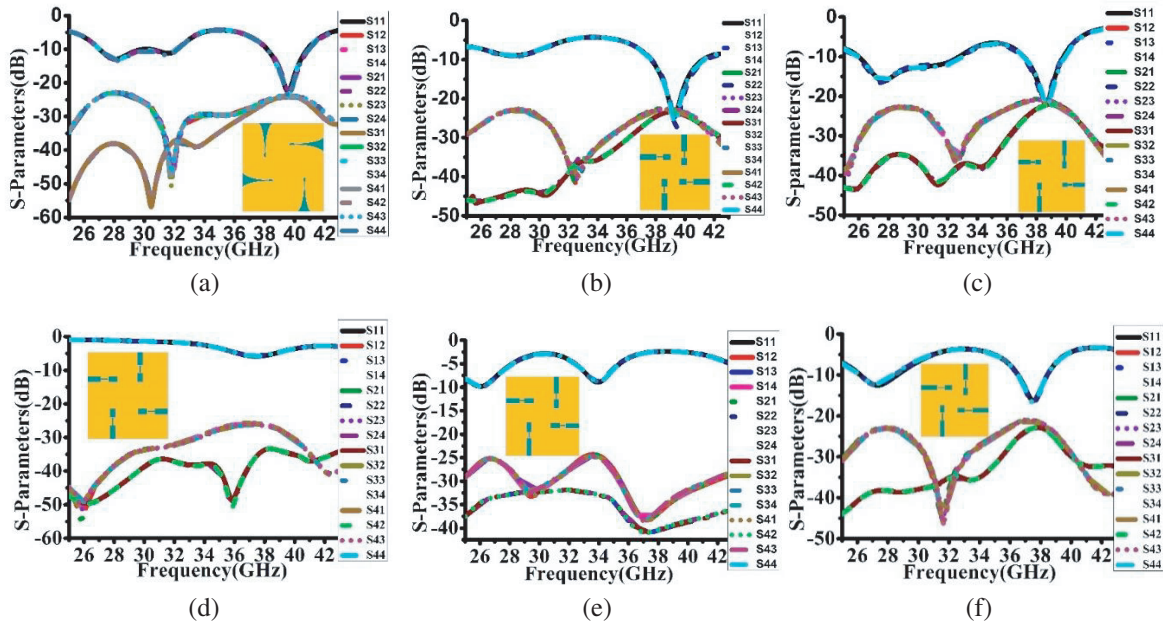


**Figure 2.** Parametric studies of proposed antenna  $S$ -parameters. (a) By varying  $W_a$ . (b) By varying  $W_1$ . (c) By varying  $W_2$ . (d) By varying  $L_1$ . (e) By varying  $L_2$ . (f) By varying  $L_3$ .

The patch impedance is determined by

$$Z_a = 90 \frac{\epsilon_r^2}{\epsilon_r - 1} \left( \frac{L}{W} \right)^2 \tag{5}$$

Transition line character impedance is obtained by following equation

$$Z_T = \sqrt{50 + Z_a} \tag{6}$$

The width of the transition line and width of the  $50\Omega$  microstrip feed line are calculated by using following equations

$$Z_T = \frac{60}{\sqrt{\epsilon_r}} \ln \left( \frac{8d}{W_T} + \frac{W_T}{4d} \right) \tag{7}$$

$$Z_0 = \frac{120\pi}{\sqrt{\varepsilon_{reff}} \left( 1.393 + \frac{W}{h} + \frac{2}{3} \ln \left( \frac{W}{h} + 1.44 \right) \right)} \quad (8)$$

The lengths of microstrip feed line and transition line are calculated using

$$R_{in(x=0)} = \cos^2 \left( \frac{\pi}{L} x_0 \right) \quad (9)$$

$$l = \frac{\lambda}{4} = \frac{\lambda_0}{4\sqrt{\varepsilon_{reff}}} \quad (10)$$

$X_0$  indicates the length of feed line, and  $l$  indicates the length of transition line. Here calculated feed line and transition line widths are 1 mm and 0.3 mm, and similarly feed line and transition line lengths are 5.5 mm and 1.63 mm. The proposed antenna is fabricated on Rogers RT/duroid 5880 material having 2.2 dielectric constant and 0.79 mm thickness. This material has uniform electrical properties over wide frequency range [34].

When aperture width ( $W_a$ ) of exponential taper curve is changed from 5 mm to 2.4 mm, return loss is reduced at 28 GHz resonant frequency as seen in Fig. 2(a). In the feedline structure when  $W_1$  is changed from 1 mm to 1.6 mm, one band is lost at 28 GHz as seen in Fig. 2(b), and when  $W_2$  is changed from 0.3 mm to 0.7 mm, resonant frequency is changed to 27 GHz as shown in Fig. 2(c). By varying  $L_1$  value from 5.5 mm to 3.5 mm, two bands are lost as seen in Fig. 2(d), and similarly by varying  $L_2$  value from 1.63 mm to 2.03 mm, two bands are lost as shown in Fig. 2(e). By varying  $L_3$  value 1.63 mm to 2.03 mm, resonant frequencies are changed as seen in Fig. 2(f). After these parametric studies, perfect dimensions are chosen.

### 3. RESULTS AND DISCUSSIONS

#### 3.1. Single Element Vivaldi Antenna Results

Before designing four-port MIMO Vivaldi antenna, a single element Vivaldi antenna is designed using ansys HFSS. Simulated results of single element Vivaldi antenna are shown below. The antenna is fabricated on Rogers RT/Duroid 5880 material having 0.79 mm thickness, and it has dimensions  $11 \times 11 \text{ mm}^2$ .

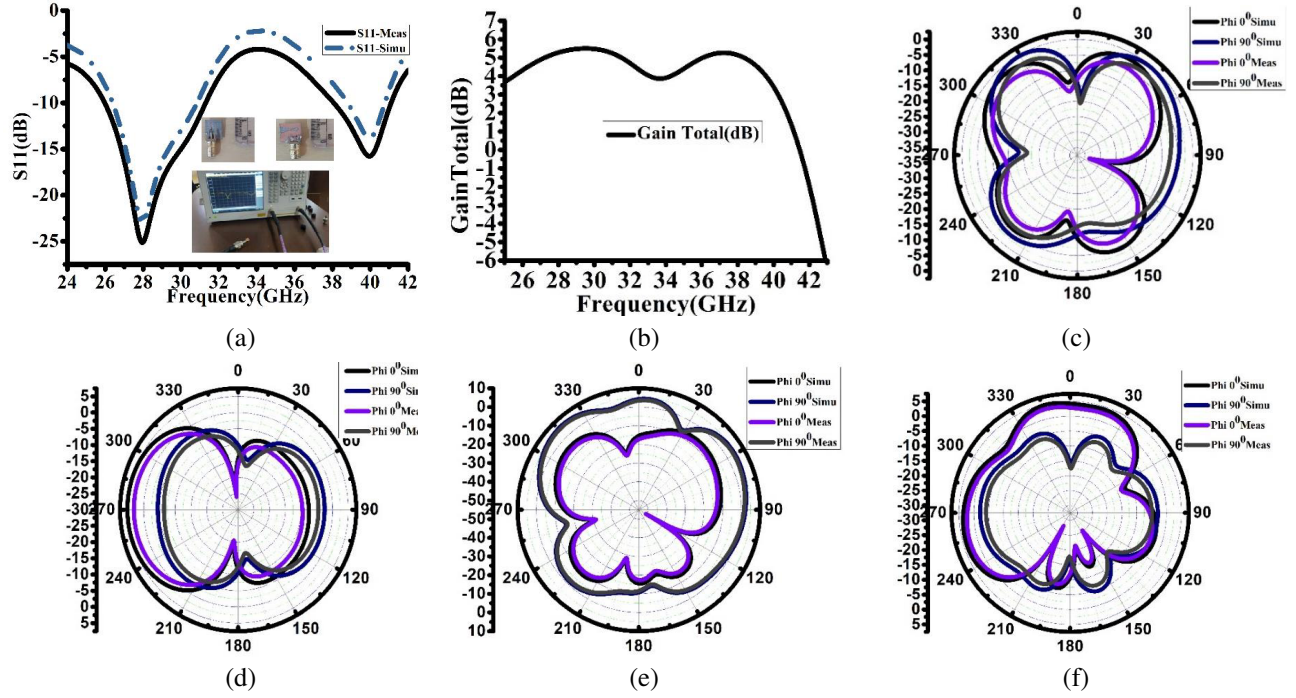
From Fig. 3, the simulated and measured results of proposed single element antenna can be observed, and the antenna resonates at two frequencies.  $S_{11}$  or return loss is below  $-10$  dB from 25.96–31.23 GHz at resonant frequency 28 GHz and occupies 5.27 GHz bandwidth. Similarly, return loss is below  $-10$  dB from 38.11 to 41.06 GHz at resonant frequency 39 GHz and occupies 2.95 GHz bandwidth which is observed in Fig. 3(a). From Fig. 3(b), the gain (Vs) frequency plot of single element antenna at dual bands can be observed. At 28 GHz 4.67 dB and at 39 GHz 4.55 dB gain is obtained. The simulated and measured results of  $E$ -plane and  $H$ -plane co- and cross-polarizations are taken at 28 GHz and 39 GHz frequencies as shown from Fig. 3(c) to Fig. 3(f).

#### 3.2. 4-Port Vivaldi MIMO Antenna Results

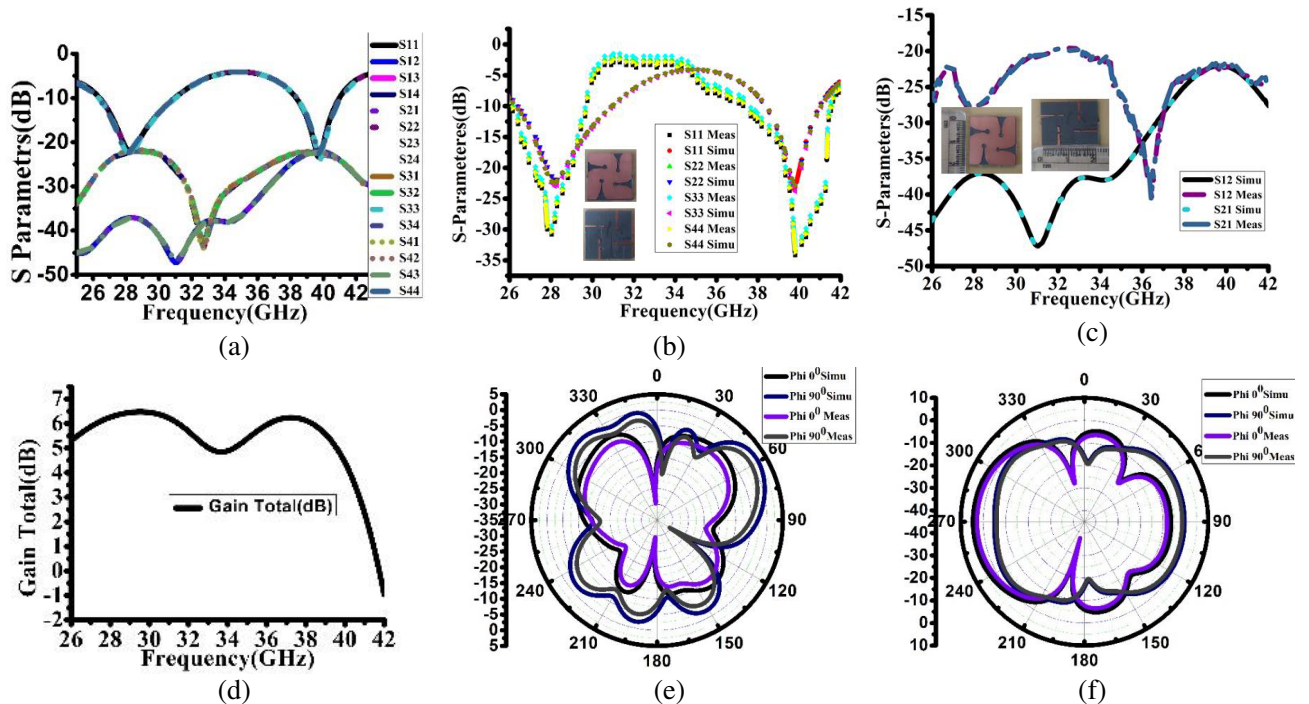
Four-port MIMO Vivaldi antenna is designed using ansys HFSS. By using MITS PCB prototyping machine, the antenna is fabricated. Fabricated results are taken using network analyzer. Far field patterns are taken using an anechoic chamber. Simulated and fabricated results are compared.

Measured and simulated results of 4-port Vivaldi MIMO antenna are represented in Fig. 4. From Fig. 4(a), the return losses of 4-elements  $S_{11}$ ,  $S_{22}$ ,  $S_{33}$ , and  $S_{44}$  are below  $-10$  dB from 26.31–30.95 GHz and 38.35–41.04 GHz. The remaining  $S$ -parameters (Isolation between antenna elements) are below  $-21.58$  dB in mentioned operating frequency bands. In Fig. 4(b) both measured and comparison plots of return loss or reflection coefficient of four antenna elements are analyzed at both the 28 GHz and 39 GHz bands, and similarly from Fig. 4(c), the comparison plot of isolation between two elements  $S_{12}$  and  $S_{21}$  can be observed. For 4-port MIMO Vivaldi antenna, the gain at 28 GHz is 5.65 dB and at 39 GHz is 5.53 dB as seen in Fig. 4(d).  $E$ -plane and  $H$ -plane co- and cross-polarizations of 4-port MIMO Vivaldi antenna simulated and measured results are taken at 28 GHz and 39 GHz as shown in

from Fig. 4(e) to Fig. 4(h). The radiation patterns are measured using an anechoic chamber as seen in Figs. 4(i) & 4(j). For reliable antenna test measurements, anechoic chambers are areas of empty space where signal reflections from nearby objects are stopped.



**Figure 3.** Single element Vivaldi antenna results. (a)  $S_{11}$  plot, (b) Gain (Vs) Frequency plot, (c)  $E$ -plane and (d)  $H$ -plane polarizations are taken at 28 GHz, (e)  $E$ -plane and (f)  $H$ -plane polarizations are taken at 39 GHz.



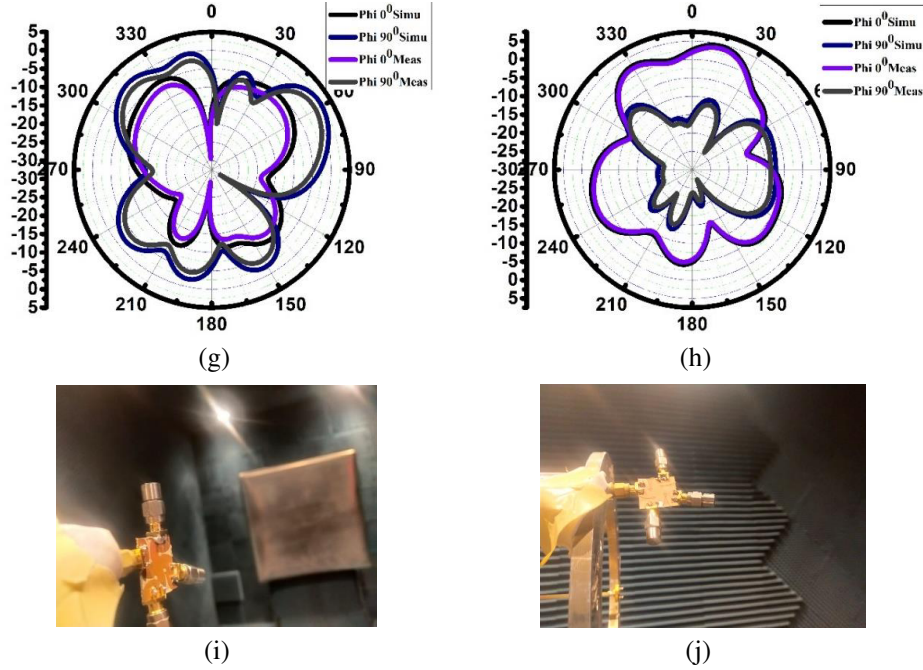


**Figure 4.** Proposed Vivaldi MIMO antenna results. (a) Simulated  $S$ -parameters plot, (b) & (c) Comparison plots of  $S$ -parameters, (d) Gain (Vs) Frequency plot, (e)  $E$ -plane and (f)  $H$ -plane polarizations are taken at 28 GHz, (g)  $E$ -plane and (h)  $H$ -plane polarizations are taken at 39 GHz, (i) & (j) Measured radiation patterns in an anechoic chamber.

### 3.3. Decoupling Mechanism of Vivaldi Antenna

The proposed decoupling concept of four-port MIMO Vivaldi antenna is based on the dismissal of the flowing currents between the antenna elements. To do this, exponential tapered curve is designed and etched on the ground surface. The suggested antenna implements the travelling wave working principle to enable current extraction and expulsion outside [29]. Therefore, ground currents can only pass longitudinally through the tapered slot and cannot pass from one antenna element to another antenna element. Observing surface current distribution can understand the proposed concept as shown in Fig. 5(a) and Fig. 5(b). From Figs. 5(a)(I)–(IV), the surface current distribution is observed at 28 GHz resonant frequency individually when port1, port2, port3, and port4 are excited. Similarly from Figs. 5(b)(I)–(IV), the surface current distribution is observed at 39 GHz resonant frequency individually when port1, port2, port3, and port4 are excited.

### 3.4. MIMO Performance Characteristics

MIMO performance characteristics like envelope correlation coefficient (ECC), diversity gain (DG), total active reflection coefficient (TARC), channel capacity loss (CCL), mean effective gain (MEG), and MEG ratio are important factors to be evaluate while analyzing MIMO antenna designs. These MIMO performance characteristics of the proposed antenna are represented from Fig. 6 to Fig. 13.

#### 3.4.1. Envelope Correlation Coefficient (ECC)

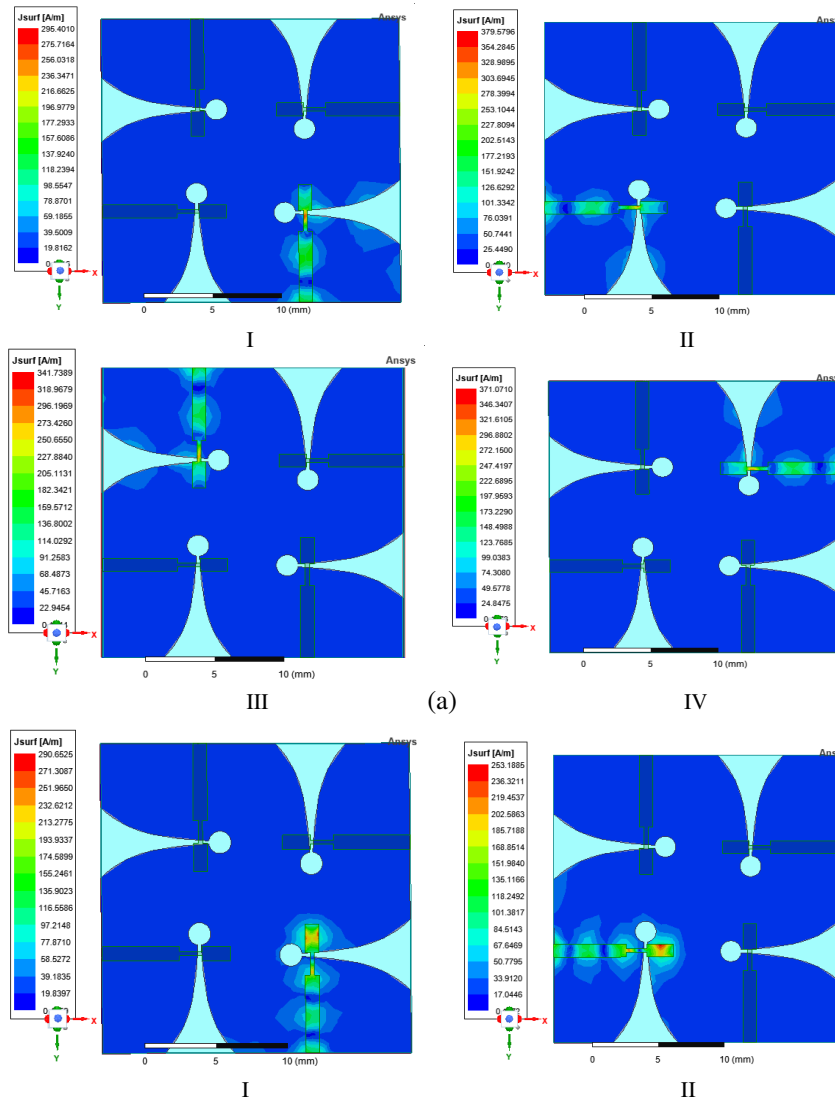
ECC is an important factor of MIMO antennas. Correlation coefficient measures independence between antenna elements, and if with any two antenna elements, one element is polarized horizontally and the other element vertically, the correlation between elements is zero. ECC can be calculated from  $S$ -parameters or from the far field patterns. By using the following formulas, ECC can be derived as

follows

$$ECC_{or\rho_{ij}} = \frac{|S_{ii}^*S_{ij} + S_{ji}^*S_{jj}|^2}{(1 - |S_{ii}|^2 - |S_{ji}|^2)(1 - |S_{jj}|^2 - |S_{ij}|^2)} \tag{11}$$

$$ECC = \frac{\left| \iint \vec{E}_1(\theta, \varphi) \cdot \vec{E}_2^*(\theta, \varphi) d\Omega \right|^2}{\iint |\vec{E}_1^*(\theta, \varphi)|^2 d\Omega \iint |\vec{E}_2(\theta, \varphi)|^2 d\Omega} \tag{12}$$

From Eq. (11), ECC can be calculated using S-parameters, and from Eq. (12), ECC can be calculated using far-field patterns. The ECC is typically determined between two antenna elements. In general, the correlation standard value is less than 0.5. In this instance, the ECC is calculated between antenna elements (1, 2), (1, 3), (1, 4), (2, 3), (2, 4), and (3, 4). In Fig. 6, it can be observed that the ECC (*S*-parameters) is obtained as less than 0.001, and in Fig. 7, it can be observed that the ECC (Far-field patterns) is obtained as less than 0.003 for mentioned frequency ranges.



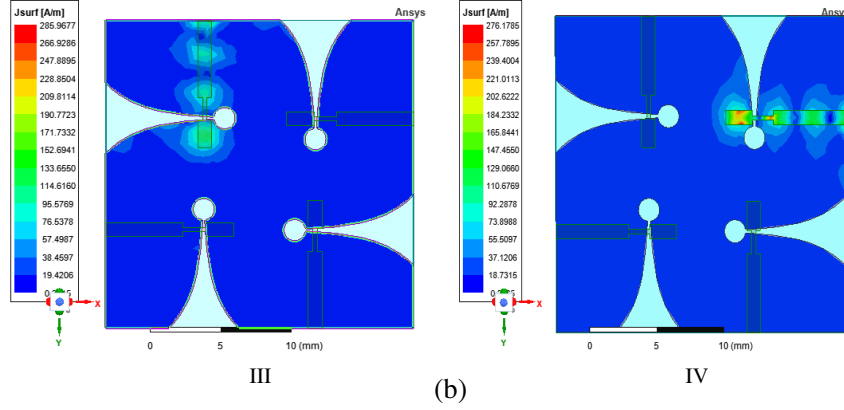


**Figure 5.** Surface current distribution of proposed 4-port Vivaldi MIMO antenna. (a) Surface current distribution of MIMO antenna at 28 GHz, (I) When port 1 is excited, (II) When port 2 is excited, (III) When port 3 is excited, (IV) When port 4 is excited. (b) Surface current distribution of MIMO antenna at 39 GHz, (I) When port 1 is excited, (II) When port 2 is excited, (III) When port 3 is excited, (IV) When port 4 is excited.

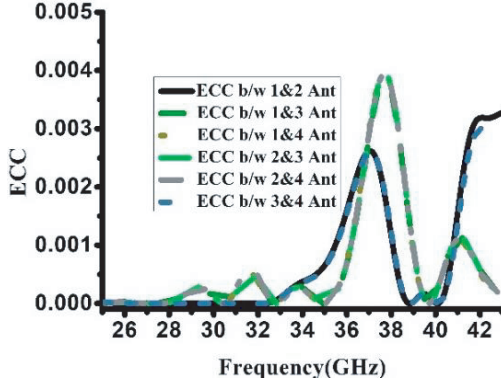


**Figure 6.** ECC-calculated from  $S$ -parameters.

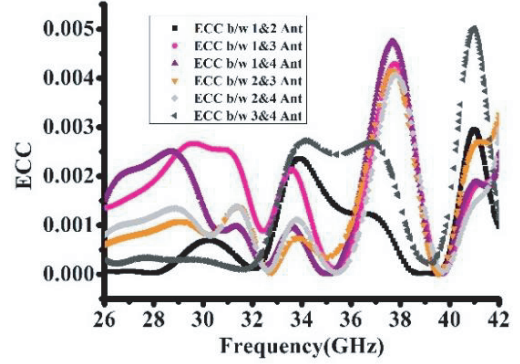


**Figure 7.** ECC-calculated from far field patterns.

### 3.4.2. Diversity Gain (DG)

The word “diversity gain” (DG) is defined as how much power is reduced in transmitted power whenever the diversity concept is applied. DG is derived from the following equation as

$$DG = 10\sqrt{1 - |\rho_{ij}|^2} \quad (13)$$

The diversity performance of the antenna is good when the MIMO antenna DG value is 10. From Fig. 8 it is seen that the diversity gain is almost equal to 10 for specified frequency ranges and is calculated among (1, 2), (1, 3), (1, 4), (2, 3), (2, 4), and (3, 4) antenna elements.

### 3.4.3. CCL (Channel Capacity Loss)

In MIMO antenna systems, the correlation effect offers information according to the channel capacity losses. The CCL practical standard value is 0.4 bits/s/Hz. Channel capacity loss can be mathematically derived as

$$C_{loss} = -\log_2 \det(\varphi^R) \quad (14)$$

$$\varphi^R = \begin{bmatrix} \rho_{11} & \rho_{12} \\ \rho_{21} & \rho_{22} \end{bmatrix} \quad (15)$$

$$\rho_{ii} = 1 - (|s_{ii}|^2 + |s_{ij}|^2) \quad \rho_{ij} = -(s_{ii}^* s_{ij} + s_{ji}^* s_{jj}) \quad (16)$$

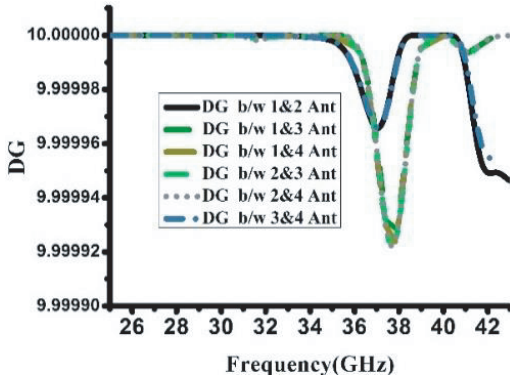


**Figure 8.** DG of Proposed MIMO Vivaldi antenna.

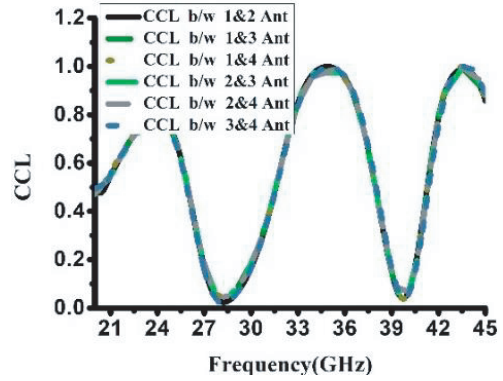


**Figure 9.** CCL of Proposed MIMO Vivaldi antenna.

where  $\varphi^R$  is the correlation matrix. Channel capacity loss is less than 0.4 bits/s/Hz for specified frequency bands as shown in Fig. 9. CCL is calculated among (1, 2), (1, 3), (1, 4), (2, 3), (2, 4), and (3, 4) antenna elements.

#### 3.4.4. Total Active Reflection Coefficient (TARC)

TARC is defined as the ratio of square root of total reflected power to the total incident power. TARC is mainly used to observe the effective reflection coefficient of MIMO systems. For  $N$ -port, the total active reflection coefficient can be defined [30] as

$$\Gamma_x^t = \frac{\sqrt{\sum_{i=1}^N |y_i|^2}}{\sqrt{\sum_{i=1}^N |x_i|^2}} \quad (17)$$

Here  $x_i$  indicates incident signal, and  $y_i$  indicates reflected signal. For 4-port MIMO antenna, the scattering matrix can be expressed as

$$\begin{bmatrix} y_1 \\ y_2 \\ y_3 \\ y_4 \end{bmatrix} = \begin{bmatrix} S_{11} & S_{12} & S_{13} & S_{14} \\ S_{21} & S_{22} & S_{23} & S_{24} \\ S_{31} & S_{32} & S_{33} & S_{34} \\ S_{41} & S_{42} & S_{43} & S_{44} \end{bmatrix} \begin{bmatrix} x_1 \\ x_2 \\ x_3 \\ x_4 \end{bmatrix} \quad (18)$$

For 4-port MIMO antenna, the total active reflection coefficient can be defined as [31, 32]

$$\Gamma_x^t = \sqrt{\frac{|(s_{11} + s_{12} + S_{13} + S_{14})|^2 + |(s_{21} + s_{22} + S_{23} + S_{24})|^2 + |(S_{31} + S_{32} + S_{33} + S_{34})|^2 + |(S_{41} + S_{42} + S_{43} + S_{44})|^2}{4}} \quad (19)$$

From Fig. 10 it is observed that TARC is below  $-10$  dB for specified frequency bands calculated among (1, 2), (1, 3), (1, 4), (2, 3), (2, 4), and (3, 4) antenna elements. The overall total active reflection coefficient is observed in Fig. 11, and for specified frequency bands,  $-10$  dB is obtained.

#### 3.4.5. Mean Effective Gain (MEG) and MEG Ratio

Mean effective gain expresses the mean received power in fading environment and is calculated individually by antenna elements. MEG is derived mathematically as [33]

$$MEG_i = 0.5\mu_{irad} = 0.5 \left( 1 \sum_{j=1}^K |s_{ij}|^2 \right) \quad (20)$$

Here  $K$  represents the number of antenna elements, and ‘ $i$ ’ is the individual antenna element. MEG value should be  $-3\text{ dB} \leq \text{MEG} < -12\text{ dB}$ . For four antenna elements, the calculated MEGs are shown in Fig. 12. For any two antenna elements if we take MEG ratio ( $\frac{\text{MEG}_i}{\text{MEG}_j}$ ), the value should be  $\leq \pm 3\text{ dB}$  and is shown in Fig. 13. The MEG ratio is calculated among (1, 2), (1, 3), (1, 4), (2, 3), (2, 4), and (3, 4) antenna elements.

A proposed antenna is compared with existing system as shown in Table 1.

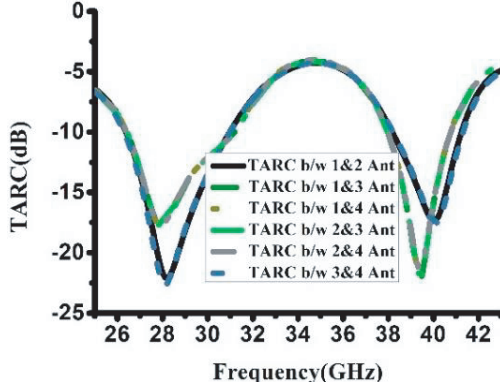


**Figure 10.** TARC between two antenna elements of proposed MIMO antenna.

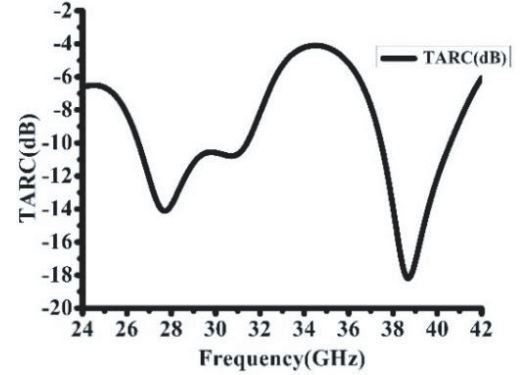


**Figure 11.** Overall TARC between antenna elements of proposed MIMO antenna.

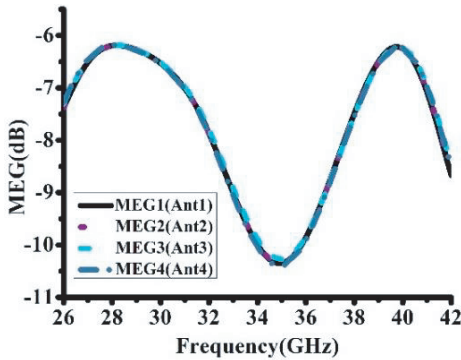


**Figure 12.** MEG of proposed MIMO antenna.

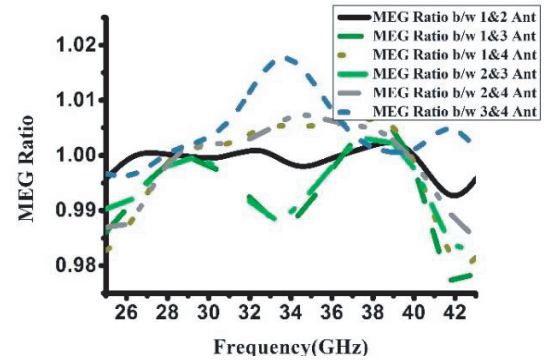


**Figure 13.** MEG ratio of proposed MIMO antenna.

**Table 1.** Comparison table of proposed antenna with existing systems.

Ref. No.	Operating Bands (GHz)	Size in mm	Bandwidth (GHz)	Gain (dB)	ECC (Using $S$ -parameters)	No. of elements
[23]	28/38	$14 \times 14$	2.4/2	8.04/6	$< 0.005$	4
[24]	28/38	$27.65 \times 12$	4/5.5	5.2/5.3	$< 0.0002$	2
[25]	28/38	$26 \times 14.5$	-	4.5/5.5	$< 0.0001$	2
[27]	28	$30 \times 35$	4.1	8.3	$< 0.04$	4
[29]	27/39	$26 \times 11$	2.7/5	5/5.7	$< 0.0001$	2
Proposed work	28/39	$22 \times 22$	4.634/2.69	5.65/5.53	$< 0.001$	4

#### 4. CONCLUSION

For 5G millimeter wave applications operating at 28 GHz and 39 GHz, a brand-new compact dual-band 4-port Vivaldi MIMO antenna is designed. A single element antenna with dimensions  $11 \times 11 \times 0.79 \text{ mm}^3$  is designed for 5G MMW applications at 28 GHz & 39 GHz bands, and further a four port MIMO Vivaldi antenna is designed. The proposed four-port Vivaldi MIMO antenna covers the frequencies of 38.35–41.04 GHz and 26.31–30.95 GHz. The 4-port antenna with dimensions  $22 \times 22 \times 0.79 \text{ mm}^3$  is fabricated on Rogers RT/Duroid, which has a 2.2 dielectric constant. For single element Vivaldi antenna, the gain is observed as 4.67 dB at 28 GHz and 4.55 dB at 39 GHz. Similarly for 4-port Vivaldi MIMO antenna, the gain is observed as 5.65 dB at 28 GHz and 5.53 dB at 39 GHz. The estimated MIMO parameters are obtained as  $\text{ECC} < 0.001$  using  $S$ -parameters,  $\text{ECC} < 0.003$  using far field patterns. DG is almost equal to 10; CCL is less than 0.4 (bits/s/Hz); overall TARC is less than  $-10$  dB; MEG is less than  $-6$  dB; and MEG ratio is less than 1.01 for the specified bands.

#### REFERENCES

1. Kumar, S., A. S. Dixit, R. R. Malekar, H. D. Raut, and L. K. Shevada, "Fifth generation antennas: A comprehensive review of design and performance enhancement techniques," *IEEE Access*, Vol. 8, 163568–163593, 2020.
2. Ericson, "Leveraging the potential of 5G millimeter wave," <https://www.ericsson.com/en/reports-and-papers/further-insights/leveraging-the-potential-of-5g-millimeter-wave>.
3. Rappaport, T. S., S. Sun, R. Mayzus, et al., "Millimeter wave mobile communications for 5G cellular: It will work!" *IEEE Access*, Vol. 1, 335–349, 2013.
4. Gibson, P. J., "The Vivaldi aerial," *1979 9th European Microwave Conference*, 101–105, 1979.
5. Gjokaj, V., J. Papapolymerou, J. D. Albrecht, B. Wright, and P. Chahal, "A compact receive module in 3-D printed Vivaldi antenna," *IEEE Transactions on Components, Packaging and Manufacturing Technology*, Vol. 10, No. 2, 343–346, Feb. 2020.
6. Shan, J., A. Xu, and J. Lin, "A parametric study of microstrip-fed Vivaldi antenna," *3rd IEEE International Conference on Computer and Communications (ICCC)*, 1099–1103, 2017.
7. Li, Z., C. Yin, and X. Zhu, "Compact UWB MIMO Vivaldi antenna with dual band-notched characteristics," *IEEE Access*, Vol. 7, 38696–38701, 2019.
8. Li, Q. and Y. Sun, "A high isolation UWB MIMO antenna based on angle diversity," *2020 IEEE MTT-S International Wireless Symposium (IWS)*, 1–3, 2020.
9. Arezoomand, A., et al., "Photonic band gap implementation for phase centre controlling in Vivaldi antenna," *IET Microwaves, Antennas & Propagation*, Vol. 11, No. 13, 1880–1886, 2017.
10. Hatami, A., A. S. Arezomand, and F. B. Zarrabi, "Phase center controlling in Vivaldi antenna: Review and development of the story," *Journal of Computational Electronics*, Vol. 19, 736–749, 2020.
11. Poorgholam-Khanjari, S. and F. B. Zarrabi, "Reconfigurable Vivaldi THz antenna based on graphene load as hyperbolic metamaterial for skin cancer spectroscopy," *Optics Communications*, Vol. 480, 126482, 2021.
12. Elsheakh, D. M. and E. A. Abdallah, "Ultrawideband Vivaldi antenna for DVB-T, WLAN and WiMAX Applications," *International Journal of Antennas and Propagation*, Vol. 2014, 2014.
13. Zhu, Y., D. Su, W. Xie, Z. Liu, and K. Zuo, "Design of a novel miniaturized Vivaldi antenna with loading resistance for Ultra Wideband (UWB) applications," *ACES Journal*, Vol. 32, No. 10, 895–900, Jul. 2021.
14. Paul, L. C. and Md. M. Islam, "A super wideband directional compact Vivaldi antenna for lower 5G satellite applications," *International Journal of Antennas and Propagation*, 2021.
15. Hasan, Md. N., S. Bashir, and S. Chu, "Dual band omnidirectional millimeter wave antenna for 5G communications," *Journal of Electromagnetic Waves and Applications*, Vol. 33, No. 12, 1581–1590, 2019.

16. Marzouk, H. M., M. I. Ahmed, and A. H. A. Shaalan, "Novel dual-band 28/38 GHz MIMO antennas for 5G mobile applications," *Progress In Electromagnetics Research C*, Vol. 93, 103–117, 2019.
17. Ali, W., S. Das, H. Medkour, and S. Lakrit, "Planar dual-band 27/39 GHz millimeter-wave MIMO antenna for 5G applications," *Microsystem Technologies*, Vol. 27, 283–292, 2021.
18. Mallat, N. K., M. Nouri, S. A. Aghdam, M. T. Zia, B. Harb, and A. Jafarieh, "A dual circularly reconfigurable polarization patch antenna for fifth generation mobile communication systems," *Progress In Electromagnetics Research C*, Vol. 105, 73–84, 2020.
19. Farahat, A. E. and K. F. A. Hussein, "Dual-band (28/38 GHz) Yagi-Uda antenna with corrugated radiator and triangular reflectors for 5G mobile phones," *The Applied Computational Electromagnetics Society Journal (ACES)*, 1325–1334, 2021.
20. El-Hassan, M. A., K. F. A. Hussein, and A. E. Farahat, "Compact dual-band (28/38 GHz) patch for MIMO antenna system of polarization diversity," *The Applied Computational Electromagnetics Society Journal (ACES)*, 716–725, 2022.
21. Farahat, A. E. and K. F. A. Hussein, "Dual-band (28/38 GHz) wideband MIMO antenna for 5G mobile applications," *IEEE Access*, Vol. 10, 32213–32223, 2022.
22. Hussain, M., W. A. Awan, E. M. Ali, et al., "Isolation improvement of parasitic element-loaded dual-band MIMO antenna for mm-wave applications," *Micromachines*, Vol. 13, No. 11, 1918, 2022.
23. Tadesse, A. D., O. P. Acharya, and S. Sahu, "A compact planar four-port MIMO antenna for 28/38 GHz millimeter-wave 5G applications," *Advanced Electromagnetics*, Vol. 11, No. 3, 16–25, 2022.
24. Sabek, A. R., W. A. E. Ali, and A. A. Ibrahim, "Minimally coupled two-element MIMO antenna with dual band (28/38 GHz) for 5G wireless communications," *Journal of Infrared, Millimeter, and Terahertz Waves*, 1–14, 2022.
25. Esmail, B. A. and S. Koziel, "High isolation metamaterial-based dual-band MIMO antenna for 5G millimeter-wave applications," *AEU — International Journal of Electronics and Communications*, Vol. 158, 154470, 2023.
26. Ikram, M., N. Nguyen-Trong, and A. M. Abbosh, "Realization of a tapered slot array as both decoupling and radiating structure for 4G/5G wireless devices," *IEEE Access*, Vol. 7, 159112–159118, 2019.
27. Khalid, M., et al., "4-port MIMO antenna with defected ground structure for 5G millimeter wave applications," *Electronics*, Vol. 9, No. 1, 71, 2020.
28. Jaiswal, P. K., R. Bhattacharya, and A. Kumar, "A UWB antipodal Vivaldi antenna with high gain using metasurface and notches," *AEU — International Journal of Electronics and Communications*, Vol. 159, 154473, 2023.
29. Tebache, S., A. Belouchrani, F. Ghanem, and A. Mansoul, "Novel reliable and practical decoupling mechanism for strongly coupled antenna arrays," *IEEE Transactions on Antennas and Propagation*, Vol. 67, No. 9, 5892–5899, Sept. 2019.
30. Fritz-Andrade, E., H. Jardon-Aguilar, and J. A. Tirado-Mendez, "The correct application of total active reflection coefficient to evaluate MIMO antenna systems and its generalization to  $N$  ports," *International J. of RF and Microwave Computer-Aided Engineering*, Vol. 30, No. 4, e22113, 2020.
31. Kumar, A., A. Q. Ansari, B. K. Kanaujia, and J. Kishor, "High isolation compact four-port MIMO antenna loaded with CSRR for multiband applications," *Frequenz*, Vol. 72, Nos. 9–10, 415–427, 2018.
32. Kumar, A., A. Q. Ansari, B. K. Kanaujia, et al., "A review on different techniques of mutual coupling reduction between elements of any MIMO antenna. Part 1: DGSs and parasitic structures," *Radio Science*, Vol. 56, No. 3, 1–25, 2021.
33. Khalid, M., S. I. Naqvi, N. Hussain, et al., "4-port MIMO antenna with defected ground structure for 5G millimeter wave applications," *Electronics*, Vol. 9, No. 1, 71, 2020.
34. Subitha, D., S. Velmurugan, M. V. Lakshmi, et al., "Development of Rogers RT/Duroid 5880 substrate-based MIMO antenna array for automotive radar applications," *Advances in Materials Science and Engineering*, Vol. 2022, 2022.